Control of Plasmaspheric Dynamics by Both Convection and Sub-Auroral Polarization Stream

J. Goldstein[1,2], B. R. Sandel[3], P. H. Reiff[1]

The long-standing hypothesis that plasmaspheric dynamics are described by superposition of corotation and solar-wind-driven sunward convection is tested via direct comparison between plasmasphere observations and simulation output. The observations consist of global plasmasphere images produced by the IMAGE extreme ultraviolet (EUV) imager during plasmasphere erosion on 2 June 2001. The simulation is a plasmapause evolution model driven by a time-varying Volland-Stern (VS) electric potential distribution. On the dawnside and much of the nightside the model matches the EUV plasmapause position to within 0.2–0.5 earth radii (R_E). Near dusk the model plasmapause is about 0.7–1.2 R_E farther out than the EUV plasmapause, suggesting that an improved model should include the duskside flow enhancement known as the sub-auroral polarization stream (SAPS). It is demonstrated that including a simplified ad-hoc SAPS potential can correct the model on the duskside.

1. Introduction

The plasmasphere is the cold (1 eV), dense (10^2–10^4 cm^{-3}) torus of plasma that occupies the inner portion of the magnetosphere out to a boundary known as the plasmapause where the density can drop by one or two orders of magnitude in less than one Earth radius (R_E). From decades of observations it is known that the plasmapause radial location moves inward during geomagnetic disturbance periods.

To explain the existence of a dense plasmasphere whose radial size decreases with geomagnetic activity, a long-standing hypothesis is that the dynamics of the plasmasphere are controlled by a superposition of an eastward corotational flow field and a (generally) sunward convective flow field that is driven by the flow of the solar wind (SW) and interplanetary magnetic field (IMF) past the magnetosphere [*Nishida*, 1966; *Brice*, 1967]. Enhancements in convection move the corotation/convection boundary inward, causing erosion of the outer plasmasphere as formerly corotating outer flux tubes are carried away in the newly strengthened convection field. The effects of convection can be mitigated by the process of inner magnetospheric shielding [*Jaggi and Wolf*, 1973]. In shielding, coupling between partial ring currents and the finite-conducting ionosphere creates an electric (E) field that counters the convection E-field.

Although it is consistent with the zero-order behavior of the plasmasphere during active times, the simple convective picture ignores some known or suspected complicating effects such as (but not limited to) ionospheric filling, inhomogeneity in ionospheric conductivity [*Wolf*, 1970], violations of the 'frozen-in-flux' condition, interchange instability at the plasmapause [*Lemaire*, 1975; *Huang et al.*, 1990], large-scale magnetic reconfiguration (e.g., during storms, substorms and/or solar-wind pressure pulses), and the sub-auroral polarization stream (SAPS) [*Foster and Burke*, 2002]. The SAPS is a strong sunward flow channel that has been observed at the inner edge of the plasma sheet in the dusk-to-early-morning MLT sector during active times and that forms as follows. The presence of a gap between the inner edges of the proton and electron plasma sheets generates strong poleward electric (E) fields in the poorly-conducting nightside sub-auroral ionosphere. These ionospheric E-fields map to a mostly radial direction in the equatorial plane, corresponding to a sunward flow near dusk. On average, the SAPS region in the ionosphere is below the auroral oval, about 3–5 degrees in latitudinal extent, and concentrated most strongly in the dusk/pre-midnight MLT sector [*Foster and Vo*, 2002]. Thus, in the equatorial plane the SAPS forms a radially-narrow ($\approx$2 R_E) flow channel bordering or overlapping the duskside and pre-midnight plasmasphere.

The IMAGE satellite extreme ultraviolet (EUV) imager [*Sandel et al.*, 2001] routinely obtains full global plasmasphere images by detecting 30.4 nm light resonantly scattered by the plasmaspheric He^+ ions. EUV's lower threshold is 40 e$^-$ cm$^{-3}\approx$4–8 He^+ cm^{-3} [*Goldstein et al.*, 2003b; *Moldwin et al.*, 2003]. The EUV images provide a means of evaluating the conventional picture of convection-driven plasmasphere dynamics. *Goldstein et al.* [2003a] used global EUV observations to study the timing of plasmasphere erosion at a single post-midnight magnetic local time (MLT), and concluded that convection dominated there, but the SAPS flow channel was very likely an important effect near dusk. In this letter the global quantitative contributions of shielded convection and SAPS are studied for an erosion event on 2 June 2001, through direct comparison between EUV images and the results of numerical plasmapause simulations. It will be shown that both convection and SAPS play major roles in plasmasphere dynamics during erosion.

2. Plasmapause Test Particle Simulation

Plasmasphere dynamics can be modeled by assuming that the plasmapause boundary is comprised of test particles subject to $E \times B$ drift. In a time-varying convection E-field the evolution of the plasmapause is modeled by the changing shape of the curve defined by the aggregate of these test particles, an approach hereinafter called the 'plasmapause test-particle' (PTP) simulation. This approach works best for steep plasmapause radial gradients; an indistinct boundary is obviously not well-represented by a single contour. The convection E-field model chosen to drive the PTP simulations is that of *Volland* [1973] and *Stern* [1975], which can be considered representative of the conventional convection-based picture to be tested in this letter. The Volland-Stern (VS) electric potential function is given by $\Phi_{VS}(r,\varphi) = -A_0\, r^\lambda \sin\varphi$. The value of λ determines the

[1] Department of Physics and Astronomy, Rice University, Houston, TX 77005 USA
[2] Now at: Space Science and Engineering Division, Southwest Research Institute, San Antonio, TX 78228 USA
[3] Lunar and Planetary Laboratory, University of Arizona, Tucson, AZ 85721 USA

0094-8276/03/$5.00

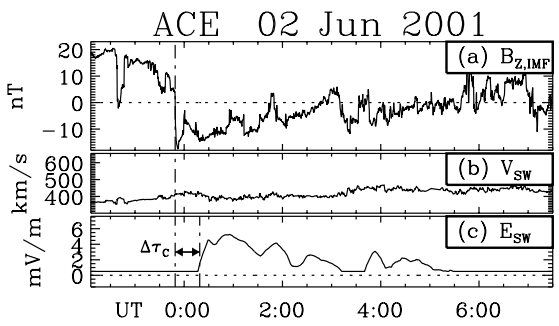

Figure 1. ACE data, 2 June 2001. (a) IMF polarity, (b) solar wind speed, (c) solar wind electric field. The southward IMF turning at 23:49 on 1 June triggered plasmaspheric erosion seen by EUV 30 minutes later.

strength of a primitive shielding effect: $\lambda = 1$ is no shielding (i.e., uniform convection E-field) and $\lambda = 2$ is the shielding value found to best agree with observations in previous studies (e.g., *Volland* [1973]; *Stern* [1975]; *Maynard and Chen* [1975]). Although the r^{λ} power law dependence is quite unrealistic at large r, and oversimplifies the shielding process (e.g., overshielding is ignored), it will be shown that the suitably normalized VS potential is not an unreasonable representation of inner magnetospheric convection. The constant A_0 is chosen so that 12 percent of the solar wind electric field is applied across the inner magnetosphere inside geosynchronous orbit: $A_0 = 0.12\,E_{\rm SW} \cdot (6.6\,R_{\rm E})^{1-\lambda}$. Assuming convection is primarily reconnection-driven during southward IMF, but that there is a finite viscous (solar-wind-magnetopause) interaction during northward IMF, the solar wind E-field is defined as the product of the solar wind speed and the southward IMF component: $E_{\rm SW} = -V_{\rm SW}\,B_{Z,\rm IMF}$, with the constraint that $E_{\rm SW} \geq 0.5\,$mV/m. The PTP simulation assumes a dipole magnetic field, a decent approximation in the inner magnetosphere for mild events. In the next section is a direct comparison between the results of this VS-driven PTP simulation and EUV images from 2 June 2001.

3. Plasmasphere Erosion, 2 June 2001

After an extended quiet (Q) period (i.e., no strong southward IMF and presumed ionospheric filling) the typical properties of the plasmasphere seen by IMAGE EUV are: (Q1) gradually decreasing density vs. radius r with no clear plasmapause boundary; (Q2) outlying plasma at large r with density near the EUV lower threshold of 4–8 $\mathrm{He^+\,cm^{-3}}$; (Q3) azimuthal density variations and irregular shape. Geomagnetic disturbance typically results in the following plasmasphere erosion (E) scenario: (E1) nightside plasmapause moves to lower r and achieves a steep radial gradient and a relatively smooth azimuthal profile; (E2) outlying nightside plasma disappears; (E3) dayside plasma moves sunward to form a broad plume. Between 0–6 UT on 2 June 2001, EUV observed erosion that commenced about 00:21 UT, apparently triggered by a southward IMF transition.

Figure 1 summarizes solar wind conditions during the first several hours of 2 June 2001, as seen by the MAG [*Smith et al.*, 1998] and SWEPAM [*McComas et al.*, 1998] instruments on the ACE spacecraft. The IMF Z-component (Figure 1(a)) and SW speed (Figure 1(b)) have been propagated to a nominal 10 $R_{\rm E}$ magnetopause from ACE's 226 $R_{\rm E}$ ($\approx$55 minutes) upstream location. Following a full day of mostly northward IMF, the IMF turned strongly southward at 23:49 UT on 1 June (the broken vertical line), producing a mild geomagnetic disturbance; although there was some substorm activity, the Dst index never dropped below -30 nT. About 32 minutes elapsed between the southward IMF turning and the earliest onset of plasmaspheric erosion seen by EUV. This as yet unexplained time delay (hereinafter called $\Delta\tau_{\rm C}$) between IMF transition and plasmasphere erosion is so far a consistent occurence in EUV observations [*Goldstein et al.*, 2003a]. The solar wind E-field in Figure 1(c) (used to drive the PTP simulation; see below) is delayed by $\Delta\tau_{\rm C}$.

Figure 3 contains EUV observations of the 2 June erosion. In each panel is an EUV image that has been mapped to the magnetic equator (see *Roelof and Skinner* [2000]; *Goldstein et al.* [2003b]; *Dent et al.* [2003]). The color scale intensity is proportional to line-of-sight integrated $\mathrm{He^+}$ column abundance. (In this letter the absolute density values are unimportant; thus no number scale is indicated in the plots.) In each panel, the PTP model plasmapause at that time is overlaid on the EUV image as a bold white curve.

The effects of plasmasphere erosion are clear in EUV image sequence 3(a)–3(d). The image in 3(a), taken at 00:01 after a day of quiet conditions, shows a typical quiet-time plasmasphere with properties (Q1)–(Q3) and a post-noon ($\sim$15 MLT) indentation or 'notch' (labeled 'N'). Figures 3(b), 3(c) and 3(d) depict plasmasphere erosion that follows (E1)–(E3). The EUV nightside plasmapause moves inward $\approx 2\,R_{\rm E}$ and becomes well-defined. Dayside plasma west of the notch moves sunward to form a broad main plume (between $Y \approx [-5, 3]\,R_{\rm E}$ at 1:43 UT). The plasma bulge east of the notch 'N' (near dusk) elongates into a thin duskside plume separated from the main plume by a narrow low-density channel that can be faintly seen as a diffuse strip of reduced EUV intensity extending outward from 'N'. In 3(d) the channel is so narrow as to be almost completely obscured.

The PTP simulation was initialized at 00:01 UT with the bold white curve in Figure 3(a), which is an isophote of the EUV image that characterizes the density gradient at the notch 'N'; it captures the size and shape of the bulk of the 00:01 UT plasmasphere but ignores the outlying density (hazy, speckled pixels near FOV edge). This initial plasmapause was allowed to evolve under the time-dependent $\lambda = 2$ Volland-Stern potential driven by $E_{\rm SW}$ of Figure 1(c). The evolution of the simulation is given by the model curves overlaid on the EUV images in Figures 3(b), 3(c) and 3(d). The overall global changes in the EUV images (inward nightside plasmapause motion, sunward dayside plasma surge) are captured by the model. In Figure 3(b) the PTP plasmapause follows the EUV well-defined nightside plasmapause to within 0.2–0.5 $R_{\rm E}$. The post-dawn hazy plasma and nightside meso-scale ($\approx$0.1–0.2 $R_{\rm E}$) plasmapause 'ripples' are not as well captured by the PTP model's one-contour approach and smooth VS potential. Near dusk, the model overestimates the Y-locations of the notch 'N' and duskside bulge (labeled 'H') by roughly

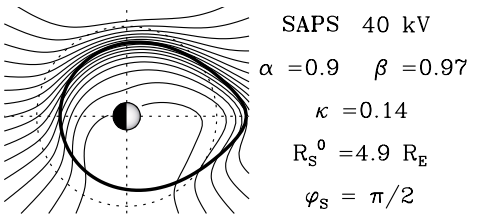

Figure 2. Equatorial 40 kV ad-hoc SAPS potential; flows are concentrated near dusk along the bold curve.

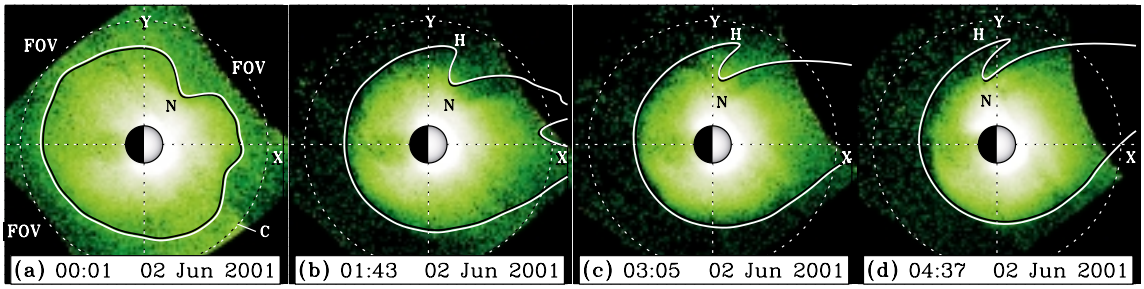

Figure 3. Four snapshots of the 2 June 2001 plasmaspheric erosion. The color images show EUV equatorial He^+ abundance. 'FOV' = edges of EUV instrument field of view. Bright patch 'C' in 3(a) is sunlight contamination, not an isolated plasma blob. The Earth is in the center, the Sun to the right. The X- and Y- axes, and geosynchronous orbit are drawn as dotted lines. The bold white traces are the model curves which mimic plasmapause gradients in EUV images; overall agreement is good except near dusk.

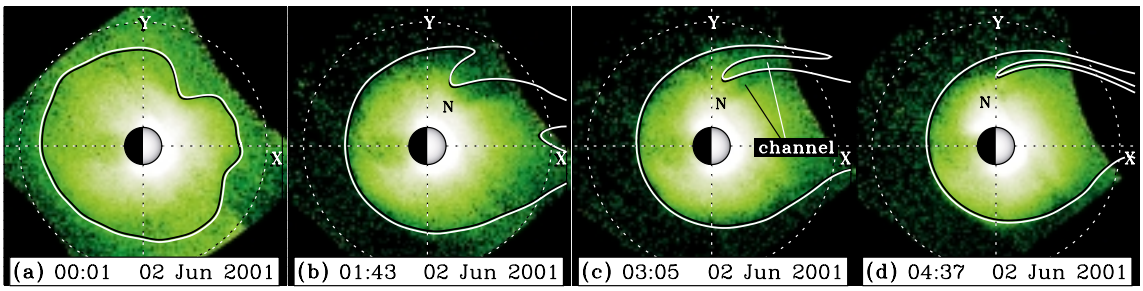

Figure 4. Model results of Figure 3 redone to include SAPS. Compare panels 4(a)–4(d) to those of Figure 3. With SAPS included, the model's duskside plasmapause is closer to observations, while the dawnside good agreement is unchanged.

0.7–1.2 R_E. In 3(c) and 3(d) the EUV dawnside plasmapause continues to be quantitatively well captured by the model. The duskside disagreement increases in 3(c) and 3(d): the model 'H' bulge stretches sunward (due to convection) into a horn-like shape, but doesn't quite elongate into a plume as happens in EUV images.

The differences between the model and the EUV images on the duskside strongly suggest that the duskside flows are too weak in the Volland-Stern model. With stronger flows near dusk, the model horn 'H' should form into a full plume as in the EUV images, and the entire plasmasphere near dusk would be smaller. Stronger duskside flows could also overpower the corotation field, causing the horn and notch to sub-corotate as they do in the EUV images. (For example, note that the MLT location of the EUV notch trails that of the model notch in 3(b) and 3(c).) One candidate to strengthen the model flows near dusk is the sub-auroral polarization stream (SAPS) introduced in section 1. Low altitude particle/flow data, recorded by the DMSP satellites on 2 June 2001, indicate a SAPS enhancement at about 1:45 UT, and a strong SAPS event 2:45–4:00 UT [J. Foster, 2003, private communication]. The time interval of the strong SAPS event (2:45–4:00 UT) coincides with the poor afternoon sector performance of the model (3(c)–3(d)). On average, SAPS strength increases gradually across the nightside from dawn (weaker) to dusk (stronger). This qualitative MLT dependence is seen in 3(d) in the size of the gap between the PTP and EUV plasmapause curves, which widens across the nightside from dawn to dusk.

4. Simulation With Ad-Hoc SAPS Model

Given the duskside disagreement between the model and EUV-observed plasmapause locations it is proposed that a more accurate inner magnetospheric E-field model can be constructed from the superposition of a shielded convection model (e.g., Volland-Stern, but for future work something with a more sophisticated shielding effect) and a SAPS model. Although no parametric model of the SAPS E-field is currently available, the statistical properties of SAPS [*Foster and Vo*, 2002] can in principle be used to construct a SAPS model that can be iteratively improved through comparison with global EUV observations.

To demonstrate the feasibility of this approach, an ad-hoc SAPS model potential was added into the PTP simulation. The equatorial potential is given by

$$\Phi_S(r,\varphi,t) = -V_S(t)\ F(r,\varphi)\ G(\varphi), \tag{1}$$

where

$$F(r,\varphi) = \tfrac{1}{2} + \tfrac{1}{\pi}\tan^{-1}\left[\,\alpha\{r - R_S(\varphi)\}\right] \tag{2}$$

$$R_S(\varphi) = R_S^0\left(\frac{1+\beta}{1+\beta\cos(\varphi-\pi)}\right)^{\kappa} \tag{3}$$

$$G(\varphi) = \cos^2\left[\tfrac{1}{2}(\varphi-\varphi_S)\right]. \tag{4}$$

This Φ_S describes a negative potential drop with a time-dependent magnitude V_S that occurs at an azimuthally-varying radius R_S. The function R_S is an ellipse-like curve (adapted from *Shue et al.* [1997]) with minimum distance R_S^0 at angle π (i.e., midnight MLT), and eccentricity governed by β and κ. The radial width of the potential drop is controlled by the α parameter in the arctangent of $F(r,\varphi)$, and the strength is modulated in local time by $G(\varphi)$, with maximum strength at φ_S. For reasonable agreement with average SAPS properties while optimizing agreement with EUV images, $[\alpha, \beta, \kappa, R_S^0, \varphi_S] = [0.9, 0.97, 0.14, 4.9R_E, \pi/2]$. The SAPS potential with these parameters and magnitude

$V_S = 40$ kV is depicted in Figure 2. The potential drop occurs along $R_S(\varphi)$ (bold curve), and is concentrated at dusk ($\varphi = \pi/2$). The simple $\cos^2$ dependence in $G(\varphi)$ gives unrealistically large SAPS flows in the pre-dusk sector, but the large SAPS radius R_S in that sector minimalizes the effect on the plasmasphere. The time-dependent strength $V_S(t)$ was chosen to very crudely represent the DMSP-deduced SAPS time profile mentioned at the end of the previous section: $V_S(t) = 40$ kV $[0.3 \exp\{-(t-1.75)^2/(1\,\mathrm{UT\,hr})^2\} + \exp\{-(t-3.38)^2/(1\,\mathrm{UT\,hr})^2\}]$.

The results of incorporating this SAPS potential into the PTP simulation of 2 June 2001 are shown in Figure 4; model plasmapause curves (bold lines) are overlaid on EUV equatorial images (color scale) in the same format as Figure 3. The inclusion of SAPS yields much better duskside agreement, and because SAPS flows are localized near dusk and pre-midnight, the dawnside good agreement is unchanged. Note that with SAPS the model horn feature of 2 June 2001 evolves correctly into a thin duskside plume separated from the main dayside plume by a thin channel.

The ad-hoc SAPS potential Φ_S is of course not accurate in a detailed sense. For example, the improved model's afternoon-sector notch ('N' in Figure 4) and low-density channel still lie eastward of the true location in the EUV images. However, the improved model performance on the duskside clearly demonstrates that simple shielded convection is quantitatively inadequate in events where SAPS are observed. The SAPS flow region can play a major role in determining the location of the duskside plasmapause and can create additional thin duskside plumes.

5. Concluding Remarks

For the 2 June 2001 plasmasphere erosion witnessed by the EUV imager, the Volland-Stern (VS) electric potential was employed in a solar-wind-driven, time-dependent plasmapause test particle (PTP) simulation. In this letter the VS potential represents the traditional convection picture, which holds that the main influences that govern plasmasphere evolution are convection and shielding (plus corotation). The routine availability of IMAGE EUV global plasmasphere images provided an excellent means to test this picture on a global scale. In this event it was found that on the dawnside and much of the nightside, the time-dependent global plasmapause shape and location can be well-described (to within a few tenths of an R_E) by a convection-based model. However, it has been demonstrated that the observed duskside plasmapause evolution may not be captured by convection alone, and that the addition of a simple ad-hoc representation of the sub-auroral polarization stream (SAPS) can in principle account for this discrepancy. Future development of this approach should involve (1) creation of a SAPS model whose spatial form and intensity are parameterized by geomagnetic activity level according to *Foster and Vo* [2002], (2) simulation of the entire plasma distribution, not just the plasmapause shape, and (3) studying the importance of additional effects such as more spatially structured convection, more realistic shielding and magnetic field, ionospheric filling, and interchange instability.

Acknowledgments. We thank N. Ness, C. Smith, D. McComas and the ACE science center for providing SW/IMF data. Work at U. Arizona supported by IMAGE program via NASA contract NAS5-96020 with SwRI. J. Goldstein supported by IMAGE grant NAS5-96020 and NASA SEC GI grant NAG5-12787.

References

Brice, N. M., Bulk motion of the magnetosphere, *J. Geophys. Res.*, *72*, 5193, 1967.

Dent, Z. C., I. R. Mann, F. W. Menk, J. Goldstein, C. R. Wilford, M. A. Clilverd, and L. G. Ozeke, A coordinated ground-based and IMAGE satellite study of quiet-time plasmaspheric density profiles, *Geophys. Res. Lett.*, *30*(12), 1600, doi:10.1029/2003GL016946, 2003.

Foster, J. C., and W. J. Burke, SAPS: A new categorization for sub-auroral electric fields, *EOS Trans. AGU*, *83*, 393, 2002.

Foster, J. C., and H. B. Vo, Average characteristics and activity dependence of the subauroral polarization stream, *J. Geophys. Res.*, *107*(A12), 1475, doi:10.1029/2002JA009409, 2002.

Goldstein, J., B. R. Sandel, W. T. Forrester, and P. H. Reiff, IMF-driven plasmasphere erosion of 10 July 2000, *Geophys. Res. Lett.*, *30*(3), doi:10.1029/2002GL016478, 2003a.

Goldstein, J., M. Spasojević, P. H. Reiff, B. R. Sandel, W. T. Forrester, D. L. Gallagher, and B. W. Reinisch, Identifying the plasmapause in IMAGE EUV data using IMAGE RPI in situ steep density gradients, *J. Geophys. Res.*, *108*(A4), 1147, doi:10.1029/2002JA009475, 2003b.

Huang, T. S., R. A. Wolf, and T. W. Hill, Interchange instability of the Earth's plasmapause, *J. Geophys. Res.*, *95*, 17,187, 1990.

Jaggi, R. K., and R. A. Wolf, Self-consistent calculation of the motion of a sheet of ions in the magnetosphere, *J. Geophys. Res.*, *78*, 2852, 1973.

Lemaire, J., The mechanisms of formation of the plasmapause, *Ann. Geophys.*, *31*, 175, 1975.

Maynard, N. C., and A. J. Chen, Isolated cold plasma regions: Observations and their relation to possible production mechanisms, *J. Geophys. Res.*, *80*, 1009, 1975.

McComas, D. J., S. J. Bame, P. Barker, W. C. Feldman, J. L. Phillips, P. Riley, and J. W. Griffee, Solar wind electron proton alpha monitor (SWEPAM) for the Advanced Composition Explorer, *Space Sci. Rev.*, *86*, 563, 1998.

Moldwin, M. B., B. R. Sandel, M. Thomsen, and R. Elphic, Quantifying global plasmaspheric images with in situ observations, *Space Sci. Rev.*, in press, 2003.

Nishida, A., Formation of plasmapause, or magnetospheric plasma knee, by the combined action of magnetospheric convection and plasma escape from the tail, *J. Geophys. Res.*, *71*, 5669, 1966.

Roelof, E. C., and A. J. Skinner, Extraction of ion distributions from magnetospheric ENA and EUV images, *Space Sci. Rev.*, *91*, 437, 2000.

Sandel, B. R., R. A. King, W. T. Forrester, D. L. Gallagher, A. L. Broadfoot, and C. C. Curtis, Initial results from the IMAGE extreme ultraviolet imager, *Geophys. Res. Lett.*, *28*, 1439, 2001.

Shue, J.-H., J. K. Chao, H. C. Fu, C. T. Russell, P. Song, K. K. Khurana, and H. J. Singer, A new functional form to study the solar wind control of the magnetopause size and shape, *J. Geophys. Res.*, *102*, 9497, 1997.

Smith, C. W., M. H. Acuna, L. F. Burlaga, J. L'Heureux, N. F. Ness, and J. Sheifele, The ACE magnetic field experiment, *Space Sci. Rev.*, *86*, 613, 1998.

Stern, D. P., The motion of a proton in the equatorial magnetosphere, *J. Geophys. Res.*, *80*, 595, 1975.

Volland, H., Semiempirical model of large-scale magnetospheric electric fields, *J. Geophys. Res.*, *78*, 171, 1973.

Wolf, R. A., Effects of ionospheric conductivity on convective flow of plasma in the magnetosphere, *J. Geophys. Res.*, *75*, 4677, 1970.

J. Goldstein, Space Sci. Division, Southwest Research Institute, San Antonio, TX 78228 USA (jerru@alum.dartmouth.org)

B. R. Sandel, Lunar and Planetary Laboratory, University of Arizona, Tucson, AZ 85721 USA

P. H. Reiff, Dept of Physics & Astronomy, Rice University, Houston, TX 77005 USA